数理解析研究所講究録
第1883巻 2014年 113-130

Numerical analysis of moving boundary problems in rarefied gas dynamics

Tetsuro Tsuji[1] and Kazuo Aoki[2]

[1]Department of Mechanical Science and Bioengineering, Osaka University
[2]Department of Mechanical Engineering and Science, Kyoto University

Abstract Motion of an infinitely wide plate in its perpendicular direction in an infinite expanse of a rarefied gas is studied numerically on the basis of the Bhatnagar-Gross-Krook model of the Boltzmann equation. The plate is subject to an external restoring force obeying Hooke's law and the drag force exerted by the surrounding gas. Thus, its motion is unsteady, and decays as time goes on due to the drag force. The motion of the plate models the decay of a linear pendulum in a rarefied gas, and the problem stated is the simplest model of a moving boundary problem in rarefied gas dynamics with mutual interaction between the motion of the plate and that of the gas. Paying attention to the singularities in the molecular velocity distribution function caused by the unsteady motion of the plate, two different numerical schemes are applied to investigate the long time behavior of the pendulum, that is, the manner of the decay.

1 Introduction

Numerical analysis of fluid flows around moving or deforming boundaries is one of the important subjects in classical fluid dynamics, and various numerical methods have been proposed and developed. As is well known, however, for gas flows in low density circumstances or in micro-scales (we call such gases rarefied gases), classical fluid dynamics cannot be applied, and kinetic theory of gases based on the Boltzmann equation has to be used. In recent years, in connection with increasing interest in gas flows around moving micro components, numerical analysis of moving-boundary problems for the Boltzmann equation has become in fashion in kinetic theory of gases. However, because of the essential difference between the equations of fluid dynamics and the Boltzmann equation, the numerical methods developed for the former equations cannot be applied directly to the Boltzmann equation. Therefore, we have to develop new numerical techniques suitable for the Boltzmann equation. For this purpose, we need to understand the basic properties of the solution of the Boltzmann equation relevant to moving-boundary problems.

In our previous paper [1], we focused our attention on this problem considering a simple spatially one-dimensional (1D) problem, i.e., an infinite plate, placed in a gas, oscillating in its normal direction. We showed that the oscillating plate generates discontinuities and other weaker singularities in the solution of the Boltzmann equation, using its Bhatnagar–Gross–Krook (BGK) model [2, 3]. We also demonstrated that the discontinuities can accumulate in a narrow range in the molecular velocity space and make the shape of the velocity distribution function highly complex. Furthermore, We have developed a numerical method (method of characteristics) for the BGK model that is capable of describing the propagation of the singularities and thus the complex shape of the velocity distribution function accurately. In the present paper, we will revisit a problem considered in [1] and investigate it more intensively.

The problem that we are going to consider is the decay of a linear pendulum in the spatially one-dimensional case. More specifically, we consider an infinite plate, placed in a rarefied gas and subject to an external restoring force obeying Hooke's law acting perpendicularly on the plate. If the plate is displaced (in its normal direction) from its equilibrium position and released, it starts, in general, an oscillatory motion. The motion then decays because of the drag force exerted by the surrounding gas. We investigate the unsteady motion of the gas caused by the oscillatory motion of the plate with special interest in the decay rate of the latter motion. Since the motion of the plate is limited to the direction perpendicular to its normal direction, we call this system a linear pendulum.

This problem has been studied for a free-molecular gas (i.e., a highly rarefied gas for which collisions between gas molecules can be neglected) [4, 5, 6] and for a special Lorentz gas (i.e., a gas interacting only with a background obstacles in a special manner) [6]. Let us denote by $X_w(t_*)$ the displacement of the plate from the equilibrium position at time t_*. Then, for a free-molecular gas, the amplitude $|X_w(t_*)|$ of oscillation of the plate decays as

$$|X_w(t_*)| \approx C t_*^{-p-1} \quad \text{for} \quad t_* \gg t_{0*}, \tag{1}$$

where t_{0*} is a reference time, C is a positive constant, and p (= 1 or 2) is an integer depending on the boundary condition on the plate. More specifically, $p = 1$ for the diffuse-reflection boundary condition [5, 6] and $p = 2$ for the specular-reflection boundary condition [4]; the former ($p = 1$) is a numerical result, whereas the latter ($p = 2$) is a theoretical one.

This power-law decay (1) is attributed to a long-memory effect caused by the molecules colliding with the plate more than once [7, 4, 8, 9, 10]. Thus, it is expected that collisions between gas molecules may destroy this long-memory effect and lead to a different manner of the decay. In fact, for the special Lorentz gas with a particular interaction with given background obstacles, the following decay was shown numerically [6]:

$$|X_w(t_*)| < C_1 \exp(-C_2 t_*) \quad \text{for} \quad t_* \gg t_{0*}, \tag{2}$$

where C_1 and C_2 are positive constants.

Our natural question is what about the decay rate when there are collisions between gas molecules. To see it numerically is the aim of the present paper. We will employ two different numerical methods: One is the method of characteristics developed in [1] and the other is the semi-Lagrangian method [11] (see the last paragraph of Sec. 2.2 for detail). We first justify the latter method by comparing its result with the accurate result based on the former method. Then, using the latter, we carry out a very long-time computation to obtain reliable results for the decay rate of the oscillation of the plate.

Remark 1: For the free-molecular gas and the special Lorentz gas, the decay of the linear pendulum has been studied also for two-dimensional (2D) and three-dimensional (3D) cases theoretically [4] and numerically [5, 6]. To be more specific, in the 2D case, the infinite plate is replaced by an infinitely long plate with a finite width, and in the 3D case, it is replaced by a circular disk with a finite radius (the thickness of the plate or the disk is assumed to be zero in [5, 6], whereas it is assumed to be finite in [4]). In 2D and 3D cases, Eq. (1) for the free-molecular gas is generalized as

$$|X_w(t_*)| \approx C t_*^{-p-d} \quad \text{for} \quad t_* \gg t_{0*}, \tag{3}$$

with $d = 1$ for the 1D case, $d = 2$ for the 2D case, and $d = 3$ for the 3D case.

Remark 2: The discontinuity of the velocity distribution function is also observed in the gas around a convex boundary (convex toward the gas region) even when the boundary is at rest and the problem is time independent. This fact was pointed out and investigated long time ago [12], and accurate numerical analysis describing the behavior of the discontinuity has been carried out [13, 14]. The propagation of discontinuities in the problem of an oscillating plate, studied in [1] and in the present paper, is closely related to the discontinuity around the convex boundary in time-independent problems, since the former is caused by the convexity of the trajectory of the plate. A mathematical study of the propagation of discontinuity in the solution of the Boltzmann equation is found in [15].

2 Description of the problem

2.1 Statement of the problem and assumptions

Based on our recent paper [1], we consider the following initial-boundary-value problem in rarefied gas dynamics. An infinitely wide plate without thickness is kept at constant temperature T_{0*} and immersed in an infinite expanse of a rarefied ideal monatomic gas at a uniform equilibrium state at rest with density ρ_{0*} and temperature T_{0*} (see Fig. 1). An external restoring force obeying Hooke's law and the drag force by the surrounding gas act on the plate in its perpendicular direction. We take X_1 axis of the Cartesian coordinate system X_i perpendicular to the plate in such a way that $X_1 = 0$ is the equilibrium position of the restoring force. To be more specific, $X_1 = X_w(t_*)$, where t_* is the time variable, is the position of the plate and it obeys the equation of motion

$$\mathrm{d}^2 X_w / \mathrm{d}t_*^2 = -\omega_*^2 X_w(t_*) - G_*(t_*)/\mathcal{M}_*, \tag{4}$$

where ω_* is the proper frequency of the external restoring force, $G_*(t_*)$ is the drag force (per unit area) and $\mathcal{M}_*$ is the density of the plate multiplied by the unit length (i.e., area density).

At the initial time $t_* = 0$, the plate is released from an initial position $X_w(0) = a_*$ and set into motion along the X_1 axis without rotation. As a result, the surrounding gas is perturbed and yields net nonzero drag force acting on the plate in X_1 direction. We investigate the subsequent gas motion together with the unsteady motion of the plate based on the following assumptions:

1. The behavior of the gas is described by the BGK model of the Boltzmann equation [2, 3].

2. The gas molecules undergo diffuse reflection on the plate. More specifically, the velocity of the reflected molecules on the boundary are distributed according to the (half-range) Maxwellian distribution being characterized by the velocity and temperature of the plate and having the density determined in such a way that there is no instantaneous net mass flow across the plate.

3. Physical quantities are independent of the X_2 and X_3 directions (one-dimensional problem).

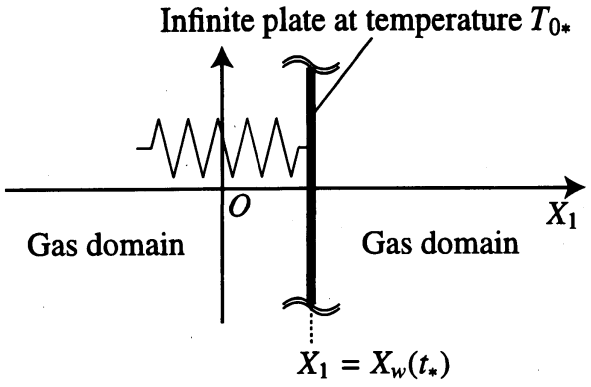

Fig. 1: Configuration of the problem.

The above-mentioned problem models a one-dimensional linear pendulum in a rarefied gas, and is a moving boundary problem with mutual interaction between the motion of the plate and that of the gas. That is, the drag force $G_*(t_*)$ acting on the plate is calculated as the net momentum fluxes on both sides of the plate (action from the gas to the plate), and the boundary condition for the BGK equation is expressed by the position and the velocity of the plate (action from the plate to the gas).

2.2 Formulation

Before presenting the basic equations, we summarize the notations used in the paper. First, we introduce (and repeat) dimensional variables: t_* is the time variable, X_i the Cartesian coordinate system in space, ξ_i the molecular velocity, X_w the position of the plate (X_1 coordinate), and V_w the velocity of the plate (X_1 direction); ρ_* is the density of the gas, u_{1*} the flow velocity of the gas in the X_1 direction (the other two components u_{2*} and u_{3*} are assumed to be zero), and T_* the temperature of the gas; G_* is the drag force acting on the plate per unit area, $\mathcal{M}_*$ the mass of the plate per unit area, a_* the initial position of the plate, and f_* the velocity distribution function of gas molecules. We choose $t_{0*} := 1/\omega_*$ and $L_{0*} := c_{0*}/\omega_*$ as, respectively, the reference time and length; $c_{0*} := \sqrt{2RT_{0*}}$ is the thermal speed at temperature T_{0*}, where R is the gas constant per unit mass ($R = k_B/m_g$ with the Boltzmann constant k_B and the mass of a gas molecule m_g). Then, we introduce the following non-dimensional variables t, x_i, ζ_i, x_w, v_w, ρ, u_1, T, G, $\mathcal{M}$, a, and f as

$$\begin{aligned} &t = t_*/t_{0*}, \quad x_i = X_i/L_{0*}, \quad \zeta_i = \xi_i/c_{0*}, \quad x_w = X_w/L_{0*}, \quad v_w = V_w/c_{0*}, \\ &\rho = \rho_*/\rho_{0*}, \quad u_1 = u_{1*}/c_{0*}, \quad T = T_*/T_{0*}, \\ &G = G_*/(\rho_{0*}c_{0*}^2), \quad \mathcal{M} = \mathcal{M}_*/(\rho_{0*}L_{0*}), \quad a = a_*/L_{0*}, \quad f = f_*/(\rho_{0*}/c_{0*}^3), \end{aligned} \tag{5}$$

In order to eliminate the molecular velocity components ζ_2 and ζ_3, we further introduce the following marginal velocity distribution functions g and h [16]:

$$\begin{bmatrix} g \\ h \end{bmatrix}(x_1, \zeta_1, t) = \int_{\mathbb{R}^2} \begin{bmatrix} 1 \\ \zeta_2^2 + \zeta_3^2 \end{bmatrix} f(x_1, \zeta_1, \zeta_2, \zeta_3, t) \mathrm{d}\zeta_2 \mathrm{d}\zeta_3. \tag{6}$$

With the variables defined above, the BGK equation is written as

$$\frac{\partial}{\partial t}\begin{bmatrix} g \\ h \end{bmatrix} + \zeta_1 \frac{\partial}{\partial x_1}\begin{bmatrix} g \\ h \end{bmatrix} = \frac{1}{\mathsf{K}}\rho\left(\begin{bmatrix} 1 \\ T \end{bmatrix} M - \begin{bmatrix} g \\ h \end{bmatrix}\right), \tag{7a}$$

$$M = \frac{\rho}{(\pi T)^{1/2}} \exp\left(-\frac{(\zeta_1 - u_1)^2}{T}\right), \quad \begin{bmatrix} \rho \\ \rho u_1 \\ 3\rho T/2 \end{bmatrix} = \int_{\mathbb{R}} \begin{bmatrix} g \\ \zeta_1 g \\ (\zeta_1 - u_1)^2 g + h \end{bmatrix} \mathrm{d}\zeta_1, \tag{7b}$$

where M is the local Maxwellian in one dimension at macroscopic density ρ, flow velocity u_1 (in x_1 direction), and temperature T; $\mathsf{K} = (\sqrt{\pi}/2) l_{0*}/L_{0*}$ is a parameter of the order of the Knudsen number $\mathrm{Kn} = l_{0*}/L_{0*}$; $l_{0*} = (2/\sqrt{\pi})(c_{0*}/A_c\rho_{0*})$ is the mean free path of gas molecules at the equilibrium stat at rest at temperature T_{0*} and density ρ_{0*}; A_c is a positive constant. The initial condition for (7) is

$$g(x_1, \zeta_1, 0) = E(\zeta_1), \quad h(x_1, \zeta_1, 0) = E(\zeta_1), \quad E(\zeta_1) := \pi^{-1/2}\exp(-\zeta_1^2). \tag{8}$$

Using the position and velocity of the plate, $x_w(t)$ and $v_w(t)$, the boundary condition on the plate is given by

$$g(x_1, \zeta_1, t) = \sigma_{w\pm}(t) E(\zeta_1 - v_w(t)), \quad h(x_1, \zeta_1, t) = \sigma_{w\pm}(t) E(\zeta_1 - v_w(t)),$$
$$\text{at} \quad x_1 = x_w(t) \pm 0, \quad \text{for} \quad \zeta_1 - v_w(t) \gtrless 0, \tag{9}$$

where

$$\sigma_{w\pm}(t) = \mp 2\sqrt{\pi} \int_{\zeta_1 - v_w(t) \lesseqgtr 0} [\zeta_1 - v_w(t)] g(x_w(t) \pm 0, \zeta_1, t) \mathrm{d}\zeta_1. \tag{10}$$

In Eqs. (9) and (10), the upper signs indicate the condition on the right surface of the plate, and the lower signs that on its left surface (see Fig. 1). The equation of motion of the plate is given by

$$\frac{\mathrm{d}x_w}{\mathrm{d}t} = v_w(t), \quad \frac{\mathrm{d}v_w}{\mathrm{d}t} = -x_w(t) - \frac{G}{\mathcal{M}}, \tag{11a}$$

$$x_w(0) = a, \quad v_w(0) = 0, \tag{11b}$$

where $\mathcal{M}$ is the density ratio between the plate and the gas and G is the drag force acting on the plate

$$G = G_+ + G_-, \quad G_\pm := \pm \int_{\mathbb{R}} [\zeta_1 - v_w(t)]^2 g(x_w(t) \pm 0, \zeta_1, t) \mathrm{d}\zeta_1. \tag{12}$$

We solve the above initial-boundary-value problem Eqs. (7)–(12) numerically by two different methods: One is the method described in [1] (the method of characteristics) and the other is the semi-Lagrangian method [11]. The former is capable of capturing the singularities inherent to the present moving boundary problem, but has a drawback in carrying out a long time computation (say, for $t > 200$) due to high numerical cost. On the other hand, the latter is suitable for a long time computation, although it is not capable of capturing the singularities. Therefore, our plan to tackle the problem is the following: We show that, in the first place, the result obtained by the semi-Lagrangian method,

which is not very accurate since it cannot capture the singularities correctly, shows the good agreement with the one obtained by the method of characteristics (accurate scheme described in [1]), provided that a long time behavior is concerned (say, for $t \approx 10^2$). Then, we use the semi-Lagrangian method to compute a very long time behavior (up to $t \approx 10^4$), which is impossible to reach by using the method of characteristics. This plan is legitimate, since the singularities decays rapidly as time goes on in the case of rarefied gas (see [1]; see also Sec. 5.1 in the present paper). Therefore, it is expected that they are not harmful (in numerical sense) when a very long time behavior is concerned. In this paper, the description of the method of characteristics is omitted since it is shown in [1] in detail, and we focus on the description of the semi-Lagrangian method in the following.

3 Preliminary for numerical analysis

3.1 Relative coordinate systems

Since Eqs. (7)–(12) is a moving boundary problem, some preliminaries make the problem simpler. Following Appendix B in [1], we introduce the space coordinate relative to $x_w(t)$ and the molecular velocity $v_w(t)$, i.e.,

$$\check{x}_1 = x_1 - x_w(t), \quad \check{\zeta}_1 = \zeta_1 - v_w(t), \quad \check{t} = t, \tag{13}$$

and introduce the new variable $\check{g}$, $\check{h}$, $\check{\rho}$, $\check{u}_1$, and $\check{T}$ as

$$\check{\mathcal{F}}(\check{x}_1, \check{\zeta}_1, \check{t}) = \mathcal{F}(\check{x}_1 + x_w(\check{t}), \check{\zeta}_1 + v_w(\check{t}), \check{t}) - E(\check{\zeta}_1 + v_w(\check{t})) \quad (\mathcal{F} = g,\ h), \tag{14a}$$

$$\check{\mathcal{H}}(\check{x}_1, \check{t}) = \mathcal{H}(\check{x}_1 + x_w(\check{t}), \check{t}) \quad (\mathcal{H} = \rho,\ T), \quad \check{u}_1(\check{x}_1, \check{t}) = u_1(\check{x}_1 + x_w(\check{t}), \check{t}) - v_w(\check{t}). \tag{14b}$$

Then, Eqs. (7)–(12) are rewritten as follows: the BGK equation

$$\left(\frac{\partial}{\partial t} + \check{\zeta}_1 \frac{\partial}{\partial \check{x}_1} - \dot{v}_w(\check{t}) \frac{\partial}{\partial \check{\zeta}_1}\right) \begin{bmatrix} \check{g} \\ \check{h} \end{bmatrix} = \frac{1}{\mathsf{K}} \begin{bmatrix} Q_g \\ Q_h \end{bmatrix} := \frac{1}{\mathsf{K}} \check{\rho} \left(\begin{bmatrix} 1 \\ \check{T} \end{bmatrix} \check{M} - \begin{bmatrix} 1 \\ 1 \end{bmatrix} E(\check{\zeta}_1 + v_w(\check{t})) - \begin{bmatrix} \check{g} \\ \check{h} \end{bmatrix} \right), \tag{15a}$$

$$\check{M} = \frac{\check{\rho}}{(\pi \check{T})^{1/2}} \exp\left(-\frac{(\check{\zeta}_1 - \check{u}_1)^2}{\check{T}}\right), \quad \begin{bmatrix} \check{\rho} \\ \check{\rho}\check{u}_1 \\ \frac{3}{2}\check{\rho}\check{T} \end{bmatrix} = \begin{bmatrix} 1 \\ -v_w(\check{t}) \\ \frac{3}{2} + v_w^2(\check{t}) - \check{\rho}\check{u}_1^2 \end{bmatrix} + \int_{\mathbb{R}} \begin{bmatrix} \check{g} \\ \check{\zeta}_1 \check{g} \\ \check{\zeta}_1^2 \check{g} + \check{h} \end{bmatrix} \mathrm{d}\check{\zeta}_1, \tag{15b}$$

the initial condition

$$\check{g}(\check{x}_1, \check{\zeta}_1, 0) = 0, \quad \check{h}(\check{x}_1, \check{\zeta}_1, 0) = 0, \tag{16}$$

the boundary condition

$$\begin{bmatrix} \check{g} \\ \check{h} \end{bmatrix} (\check{x}_1, \check{\zeta}_1, \check{t}) = \left[\check{\sigma}_{w\pm}(\check{t}) E(\check{\zeta}_1) - E(\check{\zeta}_1 + v_w(\check{t}))\right] \begin{bmatrix} 1 \\ 1 \end{bmatrix} \quad \text{at} \quad \check{x}_1 = \pm 0 \ \text{ for } \ \check{\zeta}_1 \gtrless 0, \tag{17a}$$

$$\check{\sigma}_{w\pm}(\check{t}) = \check{\sigma}_{\mathrm{eq}\pm}(v_w(\check{t})) \mp 2\sqrt{\pi} \int_{\check{\zeta}_1 \lessgtr 0} \check{\zeta}_1 \check{g}(\pm 0, \check{\zeta}_1, \check{t}) \mathrm{d}\check{\zeta}_1, \quad \left[\check{\sigma}_{\mathrm{eq}\pm}(x) := e^{-x^2} \pm x\sqrt{\pi}\mathrm{erfc}(\mp x)\right], \tag{17b}$$

and the drag force

$$G(\check{t}) = \int_{\mathbb{R}} \check{\zeta}_1^2 \check{g}(+0, \check{\zeta}_1, \check{t}) \mathrm{d}\check{\zeta}_1 - \int_{\mathbb{R}} \check{\zeta}_1^2 \check{g}(-0, \check{\zeta}_1, \check{t}) \mathrm{d}\check{\zeta}_1. \tag{18}$$

With the aid of the relative coordinate system, (15)–(18) together with Eq. (11) is the initial-boundary-value problem with a stationary boundary, and the effect of the unsteady motion of the plate appears in the third term of left hand side in Eq. (15a) as the external inertia force acting on the gas molecules. The reason why we have introduced $\check{g}$ (or $\check{h}$) as a perturbation from $E(\check{\zeta}_1 + v_w(\check{t}))$ is as follows. In the long time limit $\check{t} \to \infty$, all the quantities are supposed to approach the equilibrium values, e.g., $\lim_{\check{t}\to\infty} x_w(\check{t}) = 0$, $\lim_{\check{t}\to\infty} v_w(\check{t}) = 0$ and $\lim_{\check{t}\to\infty} g(\check{x}_1, \check{\zeta}_1, \check{t}) = E(\check{\zeta}_1 + v_w(\check{t})) = E(\check{\zeta}_1)$. Therefore, the computation of $\check{g}$ instead of g is expected to reduce numerical error for large t.

3.2 Integration along characteristics

We further introduce the characteristic form of the BGK equation (15) by integrating it along its characteristics:

$$\begin{bmatrix} \check{g} \\ \check{h} \end{bmatrix} (\check{x}_1, \check{\zeta}_1, \check{t}) = \begin{bmatrix} \check{g} \\ \check{h} \end{bmatrix} (W(\check{t}_0; \check{x}_1, \check{\zeta}_1, \check{t}), Z(\check{t}_0; \check{x}_1, \check{\zeta}_1, \check{t}), \check{t}_0) + \frac{1}{\mathsf{K}} \int_{\check{t}_0}^{\check{t}} \begin{bmatrix} Q_g \\ Q_h \end{bmatrix} (W(s; \check{x}_1, \check{\zeta}_1, \check{t}), Z(s; \check{x}_1, \check{\zeta}_1, \check{t}), s) \mathrm{d}s, \tag{19a}$$

$$W(s; \check{x}_1, \check{\zeta}_1, \check{t}) = \check{x}_1 - [\check{\zeta}_1 + v_w(\check{t})](\check{t} - s) + x_w(\check{t}) - x_w(s), \tag{19b}$$

$$Z(s; \check{x}_1, \check{\zeta}_1, \check{t}) = \check{\zeta}_1 + v_w(\check{t}) - v_w(s), \tag{19c}$$

where $\check{t}_0$ is a time in the past [see Fig. 2(a)]. The characteristic form (19) is more suitable for numerical analysis of kinetic equations since we are free from differentiating discontinuous quantity, $\check{g}$.

Furthermore, let us derive the conservation laws, which are useful in numerical analysis of the BGK equation. Multiplying Eq. (19a) by 1, $\check{\zeta}_1$, and $\check{\zeta}_1^2$ for $\check{g}$ and by 1 for $\check{h}$, and integrating in $\mathbb{R}$ with respect to $\check{\zeta}_1$, we obtain the following conservation laws (in their integral form)

$$\mathsf{M}_0 := \check{\rho} - 1 = \int_{\mathbb{R}} \check{g}(W(\check{t}_0; \check{x}_1, \check{\zeta}_1, \check{t}), Z(\check{t}_0; \check{x}_1, \check{\zeta}_1, \check{t}), \check{t}_0) \mathrm{d}\check{\zeta}_1, \tag{20a}$$

$$\mathsf{M}_1 := \check{\rho}\check{u}_1 + v_w(\check{t}) = \int_{\mathbb{R}} \check{\zeta}_1 \check{g}(W(\check{t}_0; \check{x}_1, \check{\zeta}_1, \check{t}), Z(\check{t}_0; \check{x}_1, \check{\zeta}_1, \check{t}), \check{t}_0) \mathrm{d}\check{\zeta}_1, \tag{20b}$$

$$\mathsf{M}_2 := \frac{3}{2}\check{\rho}\check{T} - \left(\frac{3}{2} + v_w^2(\check{t}) - \check{\rho}\check{u}_1^2\right) = \int_{\mathbb{R}} \check{\zeta}_1^2 \check{g}(W(\check{t}_0; \check{x}_1, \check{\zeta}_1, \check{t}), Z(\check{t}_0; \check{x}_1, \check{\zeta}_1, \check{t}), \check{t}_0) \mathrm{d}\check{\zeta}_1 + \int_{\mathbb{R}} \check{h}(W(\check{t}_0; \check{x}_1, \check{\zeta}_1, \check{t}), Z(\check{t}_0; \check{x}_1, \check{\zeta}_1, \check{t}), \check{t}_0) \mathrm{d}\check{\zeta}_1. \tag{20c}$$

The conservation laws (20) are useful in the numerical analysis in order to compute the collision term [the second term of right hand side of Eq. (19a)] implicitly (see [11]; also [17]).

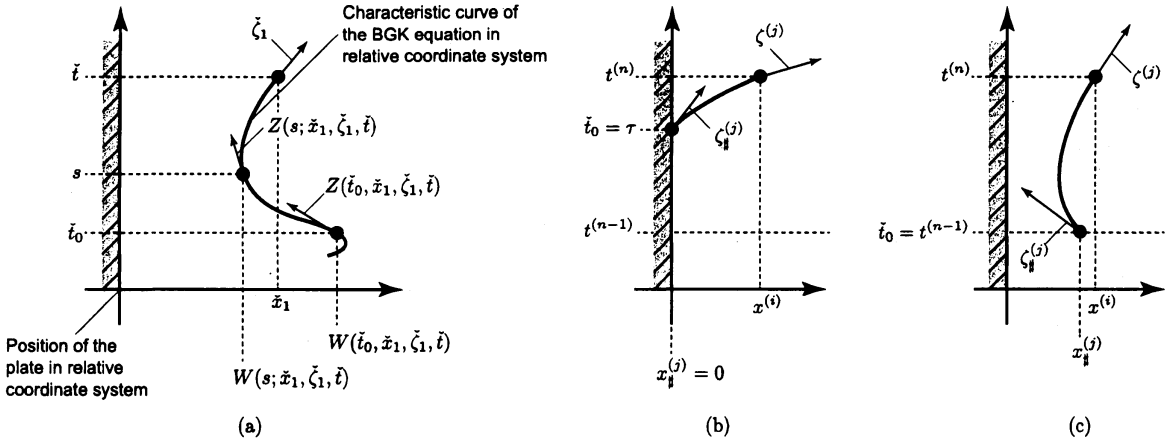

Fig. 2: Some expository figures in $(\check{x}_1, \check{t})$ plane, in which the gradient of the curve indicates the velocity. Therefore, a slope of arrow in the figure indicates the molecular velocity at the origin of the arrow. In the figure, we consider only the right half space $\check{x}_1 > 0$. (a) Illustrative figure of the characteristic form (19). For a given set of $(\check{x}_1, \check{\zeta}_1, \check{t})$, Eq. (19b) is the trajectory of a molecule in the relative coordinate system using s as a parameter. (b) Case 2 in Sec. 4.2. The characteristic curve for a given set of $(\check{x}_1, \check{\zeta}_1, \check{t})$ hits the plate at time $\tau \in [t^{(n-1)}, t^{(n)}]$. (c) Case 3 in Sec. 4.2. The characteristic curve for a given set of $(\check{x}_1, \check{\zeta}_1, \check{t})$ reaches a point in the gas domain without hitting the plate during the time interval $[t^{(n-1)}, t^{(n)}]$.

4 Numerical analysis

Since $\check{g}$ and $\check{h}$ obey the similar equations, only $\check{g}$ is discussed in this section. The following procedure is called the semi-Lagrangian method [11], since it utilizes the characteristic form (19), *keeping* $\check{t} - \check{t}_0$ *smaller than a certain value* (say, time-increment). If we let $\check{t}_0$ be a time that a characteristic curve hits a boundary (we include a line $\check{t} = 0$ as a boundary) when we traceback the molecular trajectory, then it is the method of characteristics described in [1].

4.1 Discrete variables

We introduce the discrete variables $g^{(i,j,n)}$, $U^{(i,n)}$, $t^{(n)}$, $x^{(i)}$, and $\zeta^{(j)}$, respectively, for $\check{g}$, $\check{U}$, $\check{t}$, $\check{x}_1$, and $\check{\zeta}_1$:

$$g^{(i,j,n)} = \check{g}(x^{(i)}, \zeta^{(j)}, t^{(n)}), \tag{21a}$$

$$U^{(i,n)} = \check{U}(x^{(i)}, t^{(n)}), \qquad [\check{U} = (\check{\rho}, \check{u}_1, \check{T}, \mathsf{M}_0, \mathsf{M}_1, \mathsf{M}_2)], \tag{21b}$$

$$t^{(n)}, \qquad n = 0, 1, \ldots \qquad t^{(0)} = 0, \tag{21c}$$

$$x^{(\pm i)}, \qquad i = 0, 1, \ldots, N_x, \qquad x^{(\pm 0)} = \pm 0, \tag{21d}$$

$$\zeta^{(j)}, \qquad j = -N_\zeta, \ldots, N_\zeta, \qquad \zeta^{(0)} = 0, \tag{21e}$$

and

$$x_w^{(n)} = x_w(t^{(n)}), \quad v_w^{(n)} = v_w(t^{(n)}), \quad G^{(n)} = G(t^{(n)}), \quad \sigma_{w\pm}^{(n)} = \check{\sigma}_{w\pm}(t^{(n)}). \tag{22}$$

The exact form of $x^{(\pm i)}$ and $\zeta^{(j)}$ are given in Appendix A. Moreover, the computational domain is truncated at $|\check{x}_1| = D_{\max}$ and $|\check{\zeta}_1| = Z_{\max}$, and thus we have $x^{(\pm N_x)} = \pm D_{\max}$ and $z^{(\pm N_\zeta)} = \pm Z_{\max}$. Numerical parameters $D_{\max}$ and $Z_{\max}$ are chosen suitably in such a way that the choice of these does not affect the final result. In the present paper, we set $D_{\max} = 10273$ and $Z_{\max} = 6.074$ unless otherwise stated ($N_x = 16500$ and $N_\zeta = 262$).

4.2 Flow of the numerical analysis

Suppose that everything has been obtained up to time $t^{(n-1)}$. We will give the procedure to obtain the quantities at $t^{(n)} := t^{(n-1)} + \Delta t^{(n-1)}$: $x_w^{(n)}$, $v_w^{(n)}$, $\sigma_{w\pm}^{(n)}$, $G^{(n)}$, $g^{(i,j,n)}$, $\rho^{(i,n)}$, $u_1^{(i,n)}$, and $T^{(i,n)}$. Here, $\Delta t^{(n-1)} (= t^{(n)} - t^{(n-1)})$ is not necessary a constant, e.g., it can be taken large for large n since the time variation of physical quantities such as x_w or $\check{g}$ becomes small for large time. In the present paper, $\Delta t^{(n)}$ is set to 0.01 for an initial stage, and it is gradually increased up to 0.1 as time goes on.

Our method is the so-called predictor corrector method. That is, we first compute the predicted quantities by using suitable extrapolation [see Eq. (25) below], and then we compute the corrected values without extrapolation. Predicted quantities are expressed with ˆ (hat).

(A) Obtain predicted values of the trajectory of the plate: Using Eq. (11a), compute $\hat{x}_w^{(n)}$ and $\hat{v}_w^{(n)}$ by the Euler forward method:

$$\hat{x}_w^{(n)} = x_w^{(n-1)} + \Delta t^{(n-1)} v_w^{(n-1)}, \quad \hat{v}_w^{(n)} = v_w^{(n-1)} + \Delta t^{(n-1)} \left[-x_w^{(n-1)} - \frac{G^{(n-1)}}{\mathcal{M}} \right], \tag{23}$$

and construct the cubic polynomial $\hat{\psi}^{(n-1)}(\check{t})$ that interpolates $x_w(\check{t})$ in $\check{t} \in [t^{(n-1)}, t^{(n)}]$:

$$\begin{aligned}
&\hat{\psi}^{(n-1)}(\check{t}) = \sum_{l=0}^{3} \hat{a}_{n-1,l} (\check{t} - t^{(n-1)})^l, \\
&\hat{a}_{n-1,3} = \frac{2}{[\Delta t^{(n-1)}]^3} \left(x_w^{(n-1)} - \hat{x}_w^{(n)} \right) + \frac{1}{[\Delta t^{(n-1)}]^2} \left(\hat{v}_w^{(n)} + v_w^{(n-1)} \right), \\
&\hat{a}_{n-1,2} = \frac{3}{[\Delta t^{(n-1)}]^2} \left(\hat{x}_w^{(n)} - x_w^{(n-1)} \right) - \frac{1}{\Delta t^{(n-1)}} \left(\hat{v}_w^{(n)} + 2 v_w^{(n-1)} \right), \\
&\hat{a}_{n-1,1} = v_w^{(n-1)}, \quad \hat{a}_{n-1,0} = x_w^{(n-1)}.
\end{aligned} \tag{24}$$

(B) Extrapolate some macroscopic quantities: Approximate the values on the boundary: $\hat{\sigma}_{w\pm}^{(n)}$, $\hat{\rho}^{(\pm 0,n)}$, and $\hat{T}^{(\pm 0,n)}$ as

$$\hat{\sigma}_{w\pm}^{(n)} = \check{\sigma}_{\mathrm{eq}\pm}(\hat{v}_w^{(n)}) - \check{\sigma}_{\mathrm{eq}\pm}(v_w^{(n-1)}) + \sigma_{w\pm}^{(n-1)}, \quad \hat{\rho}^{(\pm 0,n)} = \rho^{(\pm 0,n-1)}, \quad \hat{T}^{(\pm 0,n)} = T^{(\pm 0,n-1)}. \tag{25}$$

For $\hat{\sigma}_{w\pm}^{(n)}$, we partially use the updated value $\hat{v}_w^{(n)}$.

(C) Main process: This part is common for both predictor and corrector, and thus the hat representing the predictor value is omitted. The aim of this part is to compute the velocity distribution function $g^{(i,j,n)}$ (and $h^{(i,j,n)}$) by the use of Eq. (19a) and the

macroscopic quantities $\rho^{(i,n)}$, $u_1^{(i,n)}$, and $T^{(i,n)}$. First we describe the procedure to obtain the value at the "foot" of characteristic curve, i.e., $\check{g}(W(\check{t}_0;\check{x}_1,\check{\zeta}_1,\check{t}),Z(\check{t}_0;\check{x}_1,\check{\zeta}_1,\check{t}),\check{t}_0)$.

For all $i=\pm 0,...,\pm N_x$ and $j=0,...,\pm N_\zeta$ except for (i,j) such that $x^{(i)}=\pm 0$ and $\zeta^{(j)}\gtrless 0$ [(i,j) for which the boundary condition is applied], traceback the corresponding characteristic curve [Eq. (19b)] to the past and define $\check{t}_0$ as

$$\check{t}_0=\begin{cases}\tau=\max\{{}^{\exists}s\in[t^{(n-1)},t^{(n)})\mid W(s;x^{(i)},\zeta^{(j)},t^{(n)})=\pm 0\} & \text{for}\quad x^{(i)}\gtrless 0,\\ t^{(n-1)} & \text{otherwise.}\end{cases} \tag{26}$$

In other words, let $\check{t}_0=\tau\in[t^{(n-1)},t^{(n)})$ if the characteristic curve hits the plate during the time interval $[t^{(n-1)},t^{(n)})$ [see Fig. 2(b)], and let $\check{t}_0=t^{(n-1)}$ otherwise [see Fig. 2(c)]. For (i,j) such that the boundary condition is applied, we simply put $\check{t}_0=t^{(n)}$. The major difference between the semi-Lagrangian method and the method of characteristics [1] lies here: In the method of characteristics we traceback the characteristic curve until either it hits the plate or it reaches the initial time, whereas in the semi-Lagrangian method we traceback the characteristic curve up to $\check{t}=t^{(n-1)}$ at most. Note that $\check{t}_0$ is dependent on i, j, and n, but the corresponding superscripts are omitted. The equation $W(s;x^{(i)},\zeta^{(j)},t^{(n)})=\pm 0$ in Eq. (26) becomes the third-order polynomial equation if we use the approximation (24), which can be solved numerically by the Durand-Kerner method [18]. The Durand-Kerner method is more stable than the Newton method. Then, we have the position $x_\sharp^{(j)}$ and velocity $\zeta_\sharp^{(j)}$ of a gas molecule at the foot of characteristics from (19b) and (19c):

$$x_\sharp^{(j)}=W(\check{t}_0;x^{(i)},\zeta^{(j)},t^{(n)})\qquad\text{and}\qquad \zeta_\sharp^{(j)}=Z(\check{t}_0;x^{(i)},\zeta^{(j)},t^{(n)}). \tag{27}$$

In (27) and in the following, subscript $\sharp$ represents the value at the "foot" of the characteristics. Note that $(x_\sharp^{(j)},\zeta_\sharp^{(j)})$ is dependent on i and n, but the corresponding superscripts are omitted. Using $(x_\sharp^{(j)},\zeta_\sharp^{(j)})$, we compute

$$U_\sharp^{(j)}=\check{U}(x_\sharp^{(j)},\check{t}_0)\quad\text{and}\quad g_\sharp^{(j)}=\check{g}(x_\sharp^{(j)},\zeta_\sharp^{(j)},\check{t}_0), \tag{28}$$

by the following procedure.

Case 1: If $|\zeta_\sharp^{(j)}|>Z_{\max}$ or $|x_\sharp^{(j)}|>D_{\max}$, that is, if $(x_\sharp^{(j)},\zeta_\sharp^{(j)})$ is outside of the computational domain, substitute the global quantities (quantities at the initial state) into $\rho_\sharp^{(j)}$, $u_{1\sharp}^{(j)}$, $T_\sharp^{(j)}$, and $g_\sharp^{(j)}$:

$$\rho_\sharp^{(j)}=1,\quad u_{1\sharp}^{(j)}=-v_w(\check{t}_0),\quad T_\sharp^{(j)}=1,\quad g_\sharp^{(j)}=0. \tag{29}$$

Case 2: Else if $x_\sharp^{(j)}=\pm 0$ (or equivalently $\check{t}_0=\tau$), that is, the foot of characteristics is on the plate [see Fig. 19(b)], linearly interpolate macroscopic quantities ($\rho_\sharp^{(j)}$, $u_{1\sharp}^{(j)}$, and $T_\sharp^{(j)}$) and substitute the boundary condition (17), which is linearly interpolated, into the velocity distribution function $g_\sharp^{(j)}$:

$$\mathcal{H}_\sharp^{(j)}=\mathcal{H}^{(\pm 0,n)}\frac{\tau-t^{(n-1)}}{\Delta t^{(n-1)}}-\mathcal{H}^{(\pm 0,n-1)}\frac{\tau-t^{(n)}}{\Delta t^{(n-1)}}\quad(\mathcal{H}=\rho,\,T),\quad u_{1\sharp}^{(j)}=0, \tag{30}$$

$$g_\sharp^{(j)} = \sigma^\star_{w\sharp\pm} E(\zeta_\sharp^{(j)}) - E(\zeta_\sharp^{(j)} + v_w(\tau)) \quad \text{[see Eq. (17)]}, \tag{31a}$$

$$\sigma^\star_{w\sharp\pm} = \sigma^{(n)}_{w\pm} \frac{\tau - t^{(n-1)}}{\Delta t^{(n-1)}} - \sigma^{(n-1)}_{w\pm} \frac{\tau - t^{(n)}}{\Delta t^{(n-1)}}. \tag{31b}$$

When computing the predicted values, the information obtained in **(B)** is necessary at this stage [see Eqs. (30) and (31b)].

Case 3: Otherwise. That means, if $(x_\sharp^{(j)}, \zeta_\sharp^{(j)})$ is in the computational domain [see Fig. 19(c)], we can interpolate the following values

$$\rho_\sharp^{(j)} = \check{\rho}(x_\sharp^{(j)}, t^{(n-1)}), \quad u_{1\sharp}^{(j)} = \check{u}_1(x_\sharp^{(j)}, t^{(n-1)}), \quad T_\sharp^{(j)} = \check{T}(x_\sharp^{(j)}, t^{(n-1)}), \tag{32a}$$

$$g_\sharp^{(j)} = \check{g}(x_\sharp^{(j)}, \zeta_\sharp^{(j)}, t^{(n-1)}). \tag{32b}$$

by using the known quantities in the previous step $t = t^{(n-1)}$

$$\rho^{(i,n-1)}, \quad u_1^{(i,n-1)}, \quad T^{(i,n-1)}, \quad g^{(i,j,n-1)} \quad \text{for} \quad i = \pm 0, ..., \pm N_x, \quad j = 0, ..., \pm N_\zeta. \tag{33}$$

The interpolation is done by the third-order ENO interpolation [19].

Before working on (19a), we compute the macroscopic quantities at $\check{t} = t^{(n)}$ using the conservation laws (20), which can be written in discretized form as

$$\begin{aligned} \mathsf{M}_0^{(i,n)} &= \sum_{j=-N_\zeta}^{N_\zeta} \check{g}(x_\sharp^{(j)}, \zeta_\sharp^{(j)}, \check{t}_0) w^{(j)}, \quad \mathsf{M}_1^{(i,n)} = \sum_{j=-N_\zeta}^{N_\zeta} \zeta^{(j)} \check{g}(x_\sharp^{(j)}, \zeta_\sharp^{(j)}, \check{t}_0) w^{(j)}, \\ \mathsf{M}_2^{(i,n)} &= \sum_{j=-N_\zeta}^{N_\zeta} [\zeta^{(j)}]^2 \check{g}(x_\sharp^{(j)}, \zeta_\sharp^{(j)}, \check{t}_0) w^{(j)} + \sum_{j=-N_\zeta}^{N_\zeta} \check{h}(x_\sharp^{(j)}, \zeta_\sharp^{(j)}, \check{t}_0) w^{(j)}, \end{aligned} \tag{34}$$

where $w^{(j)}$ is the weight determined by the quadrature. The quadrature in the present paper is the Simpson's rule, which is also applied to (38). Then, by definition (20), we have

$$\begin{aligned} \rho^{(i,n)} &= 1 + \mathsf{M}_0^{(i,n)}, \quad u_1^{(i,n)} = \frac{1}{\rho^{(i,n)}} (\mathsf{M}_1^{(i,n)} - v_w^{(n)}), \\ T^{(i,n)} &= \frac{2}{3\rho^{(i,n)}} \left(\mathsf{M}_2^{(i,n)} + \frac{3}{2} + [v_w^{(n)}]^2 - \rho^{(i,n)} [u_1^{(i,n)}]^2 \right). \end{aligned} \tag{35}$$

In this way, we can obtain the macroscopic quantities at $\check{t} = t^{(n)}$ before computing the velocity distribution functions $\check{g}$ and $\check{h}$ at $\check{t} = t^{(n)}$ [17, 11]. Now, we discretize (19a) using

the trapezoidal rule (2nd order in time):

$$\begin{aligned} g^{(i,j,n)} =& g_\sharp^{(j)} + \gamma \left[Q_g(x_\sharp^{(j)}, \zeta_\sharp^{(j)}, \check{t}_0) + Q_g(x^{(i)}, \zeta^{(j)}, t^{(n)}) \right] \\ =& g_\sharp^{(j)} + \gamma \left\{ \rho_\sharp^{(j)} [M_\sharp^{(j)} - E(\tilde{\zeta}_\sharp^{(j)}) - g_\sharp^{(j)}] + \rho^{(i,n)} [M^{(i,j,n)} - E(\tilde{\zeta}^{(j)}) - g^{(i,j,n)}] \right\} \\ \Longrightarrow \quad g^{(i,j,n)} =& \frac{(1 - \rho_\sharp^{(j)}\gamma) g_\sharp^{(j)} + \gamma \left\{ \rho_\sharp^{(j)} \left[M_\sharp^{(j)} - E(\tilde{\zeta}_\sharp^{(j)}) \right] + \rho^{(i,n)} \left[M^{(i,j,n)} - E(\tilde{\zeta}^{(j)}) \right] \right\}}{1 + \rho^{(i,n)}\gamma} \end{aligned} \tag{36a}$$

$$\gamma = \frac{1}{\mathsf{K}} \frac{t^{(n)} - \check{t}_0}{2}, \quad \tilde{\zeta}_\sharp^{(j)} = \zeta_\sharp^{(j)} + v_w(\check{t}_0), \quad \tilde{\zeta}^{(j)} = \zeta^{(j)} + v_w(t^{(n)}) \tag{36b}$$

$$M_\sharp^{(j)} = \check{M}(x_\sharp^{(j)}, \zeta_\sharp^{(j)}, \check{t}_0), \qquad M^{(i,j,n)} = \check{M}(x^{(i)}, \zeta^{(j)}, t^{(n)}). \tag{36c}$$

The similar procedure can be applied to obtain $h^{(i,j,n)}$.

(D) Compute the boundary condition and the drag force: This part is also common for both predictor and corrector, and thus the hat representing the predictor value is omitted. We compute $\sigma_{w\pm}^{(n)}$ (17b) in the boundary condition and the drag force $G^{(n)}$:

$$\sigma_{w\pm}^{(n)} = \check{\sigma}_{\mathrm{eq}\pm}(v_w^{(n)}) \mp 2\sqrt{\pi} A_{1\pm}, \quad G^{(n)} = A_{2+} + A_{3+} - A_{2-} - A_{3-}, \tag{37}$$

where

$$A_{1\pm} = \int_{\check{\zeta}_1 \lessgtr 0} \check{\zeta}_1 \check{g}(\pm 0, \check{\zeta}_1, \check{t}) d\check{\zeta}_1 = \sum_{j=-N_\zeta}^{N_\zeta} \zeta^{(j)} g^{(\pm 0, j, n)} w^{(j)}, \tag{38a}$$

$$A_{2\pm} = \int_{\check{\zeta}_1 \lessgtr 0} \check{\zeta}_1^2 \check{g}(\pm 0, \check{\zeta}_1, \check{t}) d\check{\zeta}_1 = \sum_{j=-N_\zeta}^{N_\zeta} [\zeta^{(j)}]^2 g^{(\pm 0, j, n)} w^{(j)}, \tag{38b}$$

$$\begin{aligned} A_{3\pm} =& \int_{\check{\zeta}_1 \gtrless 0} \check{\zeta}_1^2 \check{g}(\pm 0, \check{\zeta}_1, \check{t}) d\check{\zeta}_1 = \int_{\check{\zeta}_1 \gtrless 0} \check{\zeta}_1^2 \left[\check{\sigma}_{w\pm}(\check{t}) E(\check{\zeta}_1) - E(\check{\zeta}_1 + v_w(\check{t})) \right] d\check{\zeta}_1 \quad [\because \text{Eq. (17a)}] \\ =& \frac{1}{4} [\sigma_{w\pm}^{(n)} - 1 \pm \mathrm{erf}(v_w^{(n)})] \pm \frac{v_w^{(n)}}{2\sqrt{\pi}} \exp(-[v_w^{(n)}]^2) - \frac{[v_w^{(n)}]^2}{2} \mathrm{erfc}(\pm v_w^{(n)}). \end{aligned} \tag{38c}$$

(E) Obtain corrected values of the trajectory of the plate: Once $\hat{G}^{(n)}$ is obtained, we can compute the corrected values of $x_w^{(n)}$ and $v_w^{(n)}$ by the use of the trapezoidal rule:

$$x_w^{(n)} = x_w^{(n-1)} + \Delta t^{(n-1)} \frac{\hat{v}_w^{(n)} + v_w^{(n-1)}}{2}, \tag{39a}$$

$$v_w^{(n)} = v_w^{(n-1)} + \Delta t^{(n-1)} \frac{1}{2} \left[-\hat{x}_w^{(n)} - \frac{\hat{G}^{(n)}}{\mathcal{M}} - x_w^{(n-1)} - \frac{G^{(n-1)}}{\mathcal{M}} \right], \tag{39b}$$

and construct the cubic polynomial $\psi^{(n-1)}$ (for corrector) that interpolates $x_w(\check{t})$ for $\check{t} \in [t^{(n-1)}, t^{(n)}]$ as in **(A)**.

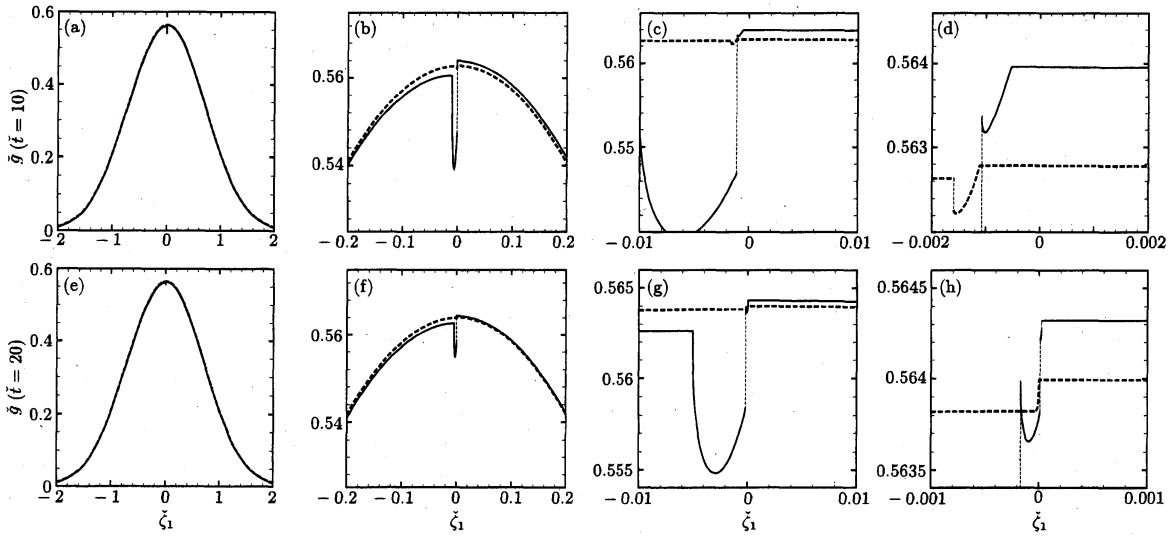

Fig. 3: Snapshot of the velocity distribution function $\check{g}(\check{x}_1, \check{\zeta}_1, \check{t})$ versus $\check{\zeta}_1$ at $\check{x}_1 = +0$ (right side of the plate) for $\mathsf{K} = 10$ (*solid line*) and $\mathsf{K} = 1$ (*dashed line*); parameters are set to $a = 0.1$ and $\mathcal{M} = 2$. Panel (a): $\check{t} = 10$. Panels (b), (c), and (d) are, respectively, closeups of panels (a), (b), and (c). Panel (e): $\check{t} = 20$. Panels (f), (g), and (h) are, respectively, closeups of panels (e), (f), and (g).

(F) Repeat the procedures (C) and (D): Note that, in obtaining corrected values, we can skip the extrapolation **(B)**, since $\hat{\sigma}_{w\pm}^{(n)}$, $\hat{\rho}^{(\pm 0,n)}$, and $\hat{T}^{(\pm 0,n)}$ are already obtained in **(C)** and **(D)** when we compute the predicted values.

5 Numerical results

In this section, the numerical results obtained by the two methods are presented. First, the method of characteristics [1] is used to investigate the singularities inherent to moving boundary problems (Sec. 5.1). Then, we compare the results obtained by the two methods through the behavior of the plate (Sec. 5.2) for a large time $\check{t} > 10^2$. Finally, the semi-Lagrangian method is used to investigate the very long time (up to $\check{t} = 10^4$) behavior of $|x_w(t)|$ (Sec. 5.3).

5.1 Velocity distribution function

We show in Fig. 3 the velocity distribution function obtained by the method of characteristics [1] for $a = 0.1$ and $\mathcal{M} = 2$. The marginal velocity distribution function $\check{g}(\check{x}_1, \check{\zeta}_1, \check{t})$ at $\check{x}_1 = +0$ (right side of the plate), $\check{t} = 10$ [Fig. 3(a)–(d)], $\check{t} = 20$ [Fig. 3(e)–(h)] are shown for $\mathsf{K} = 10$ (*solid line*) and $\mathsf{K} = 1$ (*dashed line*). Figure 3(b) [or (f)], (c) [or (g)], and (d) [or (h)] are, respectively, closeups of panels (a) [or (e)], (b) [or (f)], and (c) [or (g)] around $\check{\zeta}_1 = 0$.

To begin with, let us summarize the features of the velocity distribution function in moving boundary problems (see [1]):

F1 The velocity distribution function has several discontinuities (and also the discontinuity of the derivative with respect to $\check{\zeta}_1$) depending on the trajectory of the plate.

F2 These discontinuities accumulate around $\check{\zeta}_1 = 0$ as time goes on (localization).

F3 The derivative of the velocity distribution function with respect to $\check{\zeta}_1$ (i.e., $|\partial\check{g}/\partial\check{\zeta}_1|$) at the discontinuity may be large.

F4 The discontinuity decays as time goes on; the speed of the decay is heuristically estimated as

$$\text{Magnitude of the discontinuity} \sim \exp(-C\check{t}/\mathsf{K}), \tag{40}$$

where C is the minimum of $\check{\rho}$ along the molecular trajectory.

As one can see from Fig. 3(b)–(d) and (f)–(h), the velocity distribution function for $\mathsf{K} = 10$ is discontinuous. Moreover, in Fig. 3(h), one can see that there are several discontinuities (feature **F1**) at a couple of molecular velocities around $\check{\zeta}_1 \approx 0$ (feature **F2**). The gradient $|\partial\check{g}/\partial\check{\zeta}_1|$ is steep at some points in the case of $\mathsf{K} = 10$, e.g., $\check{\zeta}_1 \approx -0.001$ in panel(d), $\check{\zeta}_1 \approx -0.005$ in panel(g), and $\check{\zeta}_1 \approx -0.00016$ in panel(h) (feature **F3**). These steep gradients actually diverge when $\mathsf{K} \to \infty$ (weak singularity, see [1]). On the other hand, in the case of intermediate Knudsen number, $\mathsf{K} = 1$, we hardly see the discontinuities because frequent collisions between gas molecules make discontinuities smaller (feature **F4**). In addition, by comparing the curves for $\mathsf{K} = 10$ in panels (b) ($\check{t} = 10$) and (f) ($\check{t} = 20$), we notice that the discontinuity becomes smaller (feature **F4**). Note that we still see the steep gradient in Fig. 3(h) even for the case of $\mathsf{K} = 1$, although its variation is small (it is about 2×10^{-4}).

5.2 Comparison between the two methods

In Sec. 5.1, we have observed that the velocity distribution function takes the complex shape, which the semi-Lagrangian method presented in this paper is not able to reproduce. However, as one can see from Fig. 3, the magnitude of discontinuities shrink for larger $\check{t}$ and/or smaller K (feature **F4**). Therefore, we expect that the macroscopic quantities such as the drag G may not suffer from the discontinuity for larger $\check{t}$ and/or smaller K. Figure 4 demonstrates this observation. The amplitude $|x_w|$ and the speed $|v_w(t)|$ of the pendulum are plotted against $\check{t}$ in double-logarithmic scale for $\mathsf{K} = 1$, $a = 0.1$, and $\mathcal{M} = 2$. The result obtained by the semi-Lagrangian method (*solid line*) shows good agreement with that by the method of characteristics (*bold dashed* line). We conclude from Fig. 4 and the discussion in Sec. 5.1 that the semi-Lagrangian method is applicable to the long time computation of the linear pendulum.

5.3 Long time behavior

Finally, we show the long time behavior of the linear pendulum. Let us introduce the auxiliary quantity $\alpha(x_w)$ as

$$\alpha(x_w) = \frac{\mathrm{d}\log|x_w|}{\mathrm{d}\log\check{t}}. \tag{41}$$

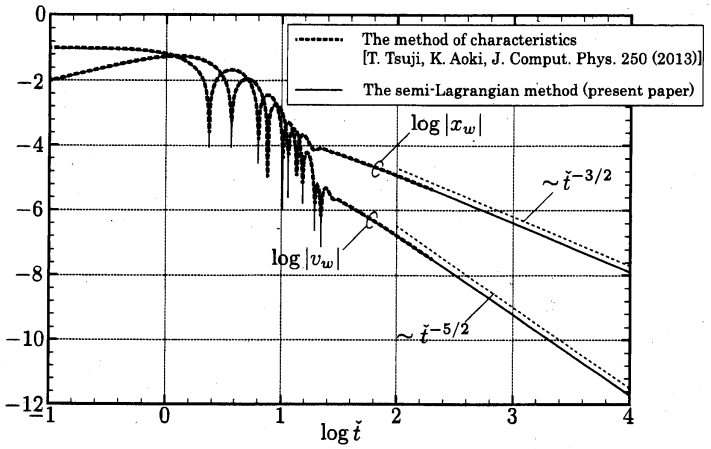

Fig. 4: Comparison between the result obtained by the method of characteristics [1] (*bold dashed line*) and that by the semi-Lagrangian method (*solid line*; see Sec. 4). The amplitude $|x_w(t)|$ and the speed $|v_w(t)|$ are shown in double-logarithmic scale. Functions proportional to $\check{t}^{-3/2}$ and $\check{t}^{-5/2}$ are also shown by *dashed line*.

The quantity $\alpha(x_w)$ corresponds to an exponent of $|x_w|$, namely, if $|x_w| \sim \check{t}^{-n}$, then we have $\alpha(x_w) = -n$. In Fig. 5, panels (a), (c), and (e) show the amplitude $|x_w|$ versus $\check{t}$ in double-logarithmic scale; panels (b), (d), and (f) show, respectively, the quantity $\alpha(x_w)$ versus $\log \check{t}$ for (a), (c), and (e). There are three physical parameters in the present problem: K, the parameter of the order of the Knudsen number, $\mathcal{M}$, the density of the mass of the plate divided by the density of the gas, and a, the initial displacement. We fix $a = 0.1$, and vary K as $\mathsf{K} = 0.4$, 1, 2, and 5; $\mathcal{M}$ as $\mathcal{M} = 2$ [Fig. 5(a)(b)], 1 [Fig. 5(c)(d)], and 0.5 [Fig. 5(e)(f)].

One can see from Fig. 5(a)(c)(e) that, for all the cases, the amplitude $|x_w|$ seems to decrease in proportion to an inverse power of time with the law

$$|x_w| \approx C\check{t}^{-3/2} \quad \text{for} \quad \check{t} \gg 1, \tag{42}$$

where C is a positive constant. In fact, it is seen that for all the cases [except for $\mathsf{K} = 0.4$ in Fig. 5(b)] the $\alpha(x_w)$ approaches $-3/2$. However, if one closely look at panels (b), (d), and (f) for the cases with $\mathsf{K} = 0.4$ and 1, the curves touch the line $-3/2$ near $\log \check{t} = 4$, i.e., these curves overshoot the value $-3/2$ [$\mathsf{K} = 0.4$ in Fig. 5(b) is clear to see this overshoot]. The cause of the overshoot is under investigation, although we observed that the overshoot tends to be suppressed for larger K and smaller $\mathcal{M}$. We have checked that, for coarser grid systems, the approach of $\alpha(x_w)$ to $-3/2$ becomes worse.

The half-integer power law decay (42) for a rarefied gas is different from either the manner of the decay for the free-molecular gas (1) or that for the special Lorentz gas (2). This indicates that the motion of the plate gives rise to another type of long-memory in the gas, which lasts longer than the long-memory of the free-molecular gas.

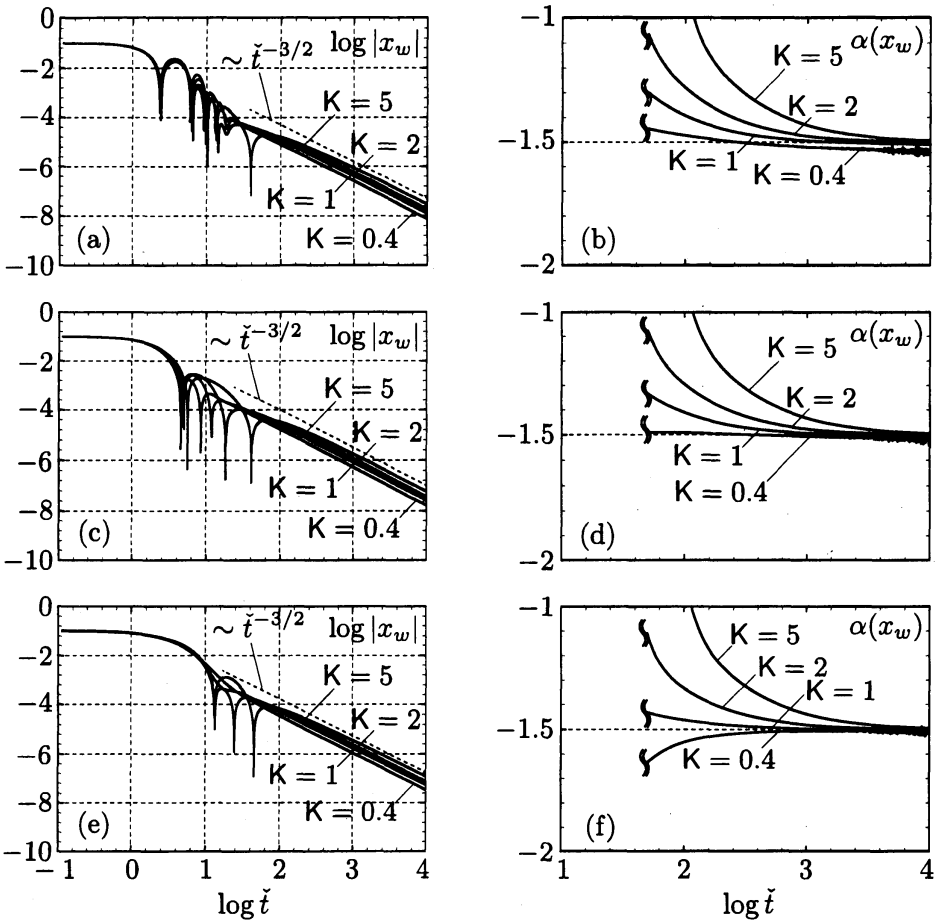

Fig. 5: The long time behaviors of the amplitude $|x_w|$ versus $\check{t}$ in double-logarithmic scale up to $\check{t} = 10^4$ for $a = 0.1$; for several K = 0.4, 1, 2, 5 and $\mathcal{M} = 2$ [panel (a)], $\mathcal{M} = 1$ [panel (c)], $\mathcal{M} = 0.5$ [panels (e)]. Panels (b), (d), and (f) show, respectively, the gradient of curves in panels (a), (c), and (e).

6 Concluding remarks

In the present paper, the motion of a model linear pendulum in a rarefied gas is investigated on the basis of the BGK model of the Boltzmann equation. This is a typical moving boundary problem in rarefied gas dynamics. The features of the velocity distribution function in the moving boundary problem, which was discussed in detail in [1], are observed by the method of characteristics. A semi-Lagrangian method is developed to solve the same problem, and it is shown that the long time behavior (up to $\check{t} \approx 10^2$) of the linear pendulum obtained by the semi-Lagrangian method is in good agreement with that obtained by the method of characteristics. By using the semi-Lagrangian method, the very long time behavior up to $\check{t} = 10^4$ of the linear pendulum, i.e., the manner of the decay of the pendulum for $\check{t} \gg 1$, is investigated. The manner of the decay seems to be described as $|x_w| \approx C\check{t}^{-3/2}$ (C is a positive constant), although more detailed analysis is necessary for more definite conclusion.

It should be mentioned that the decay rate of a linear pendulum (a sphere subject

to an external restoring force) in a Stokes fluid was proved to be $|x_w| \approx C\check{t}^{-3/2}$ in [20]. Therefore, the study of the present problem in the limit of $\mathsf{K} \to 0$ would be another interesting problem in rarefied gas dynamics.

A Grid systems

In the present paper, we use the following non-uniform grid systems for $x^{(i)}$ and $\zeta^{(j)}$. They are determined in such a way that the grid size is small when $|i|$ (or $|j|$) is small and approach a certain value when $|i|$ (or $|j|$) becomes large. The grid system for space variable $x^{(i)}$ is determined by

$$x^{(i)} = \frac{i}{|i|} a_x \left(|i| - b_x + \frac{b_x^2}{|i| + b_x} \right) \quad \text{for} \quad i \neq 0, \quad x^{(0)} = 0, \tag{43}$$

where $a_x = 1$ and $b_x = 9999$ for a reference grid. The grid system for velocity space variable $\zeta^{(j)}$ is determined by

$$\zeta^{(j)} = \begin{cases} \frac{j}{|j|} a_\zeta \left(|j| - b_\zeta + \frac{b_\zeta^2}{|j|+b_\zeta} \right) & \text{for} \quad \text{even } j \\ \frac{1}{2}(\zeta^{(j+1)} + \zeta^{(j-1)}) & \text{for} \quad \text{odd } j \\ 0 \quad \text{for} \quad j = 0 \end{cases} \tag{44}$$

where $a_\zeta = 0.2$ and $b_\zeta = 1998$ for a reference grid. We use the above values of a_x, b_x, a_ζ, and b_ζ unless otherwise stated. The value of a_x (or a_ζ) controls the grid size for $|i| \to \infty$ (or $|j| \to \infty$), and the value of b_x (or b_ζ) controls the ratio between a_x and the smallest grid size (e.g., $x^{(1)} - x^{(0)}$). As stated in the main text, when $N_x = 16500$ and $N_\zeta = 262$, we have $D_{\max} = 10273$ and $Z_{\max} = 6.074$. For these parameters, the smallest grid sizes are $x^{(1)} - x^{(0)} = 1 \times 10^{-4}$ and $\zeta^{(1)} - \zeta^{(0)} = 2 \times 10^{-4}$, and the largest grid sizes are $x^{(N_x)} - x^{(N_x-1)} = 8.576 \times 10^{-1}$ and $\zeta^{(N_\zeta)} - \zeta^{(N_\zeta-1)} = 4.354 \times 10^{-2}$.

[1] T. Tsuji, K. Aoki, Moving boundary problems for a rarefied gas: Spatially one-dimensional case, J. Comput. Phys. **250**, 574–600 (2013).

[2] P.L. Bhatnagar, E.P. Gross, M. Krook, A model for collision processes in gases. I. Small amplitude processes in charged and neutral one-component systems, Phys. Rev. **94**, 511–525 (1954).

[3] P. Welander, On the temperature jump in a rarefied gas, Ark. Fys. **7**, 507–553 (1954).

[4] S. Caprino, G. Cavallaro, C. Marchioro, On a microscopic model of viscous friction, Math. Models Methods Appl. Sci. **17**,1369–1403 (2007).

[5] T. Tsuji, K. Aoki, Decay of an oscillating plate in a free-molecular gas, in: D.A. Levin, I.J. Wysong, A.L. Garcia (Eds.), 27th International Symposium on Rarefied Gas Dynamics, 2010, AIP Conf. Proc. 1333, AIP, Melville, 2011, pp. 140–145.

[6] T. Tsuji, K. Aoki, Decay of a linear pendulum in a free-molecular gas and in a special Lorentz gas, J. Stat. Phys. **146**, 620–645 (2012).

[7] S. Caprino, C. Marchioro, M. Pulvirenti, Approach to equilibrium in a microscopic model of friction, Comm. Math. Phys. **264**, 167–189 (2006).

[8] G. Cavallaro, On the motion of a convex body interacting with a perfect gas in the mean-field approximation, Rend. Mat. Appl. **27**, 123–145 (2007).

[9] K. Aoki, G. Cavallaro, C. Marchioro, M. Pulvirenti, On the motion of a body in thermal equilibrium immersed in a perfect gas, Math. Model. Numer. Anal. **42**, 263–275 (2008).

[10] K. Aoki, T. Tsuji, G. Cavallaro, Approach to steady motion of a plate moving in a free-molecular gas under a constant external force, Phys. Rev. E **80**, 016309 1–13 (2009).

[11] G. Russo, F. Filbet, Semilagrangian schemes applied to moving boundary problems for the BGK model of rarefied gas dynamics, Kinet. Relat. Models **2**, 231–250 (2009).

[12] Y. Sone, S. Takata, Discontinuity of the velocity distribution function in a rarefied gas around a convex body and the S layer at the bottom of the Knudsen layer, Transp. Theory Stat. Phys. **21**, 501–530 (1992).

[13] H. Sugimoto and Y. Sone, Numerical Analysis of Steady Flows of a Gas Evaporating from Its Cylindrical Condensed Phase on the Basis of Kinetic Theory, Phys. Fluids A, **4**, 419–440 (1992).

[14] Y. Sone and H. Sugimoto : Kinetic Theory Analysis of Steady Evaporating Flows from a Spherical Condensed Phase into a Vacuum, Phys. Fluids A, **5**, 1491–1511 (1993).

[15] C. Kim, Formation and propagation of discontinuity for Boltzmann equation in non-convex domains, Commun. Math. Phys. **308**, 641–701 (2011).

[16] C.K. Chu, Kinetic-theoretic description of the formation of a shock wave, Phys. Fluids **8**, 12–22 (1965).

[17] F. Coron, B. Perthame, Numerical passage from kinetic to fluid equations, SIAM J. Numer. Anal. **28**, 26–42 (1991).

[18] O. Aberth, Iteration methods for finding all zeros of a polynomial simultaneously, Math. Comp. **27**, 339–344 (1973).

[19] C.-W. Shu, Essentially non-oscillatory and weighted essentially non-oscillatory schemes for hyperbolic conservation laws, in: B. Cockburn, C. Johnson, C.-W. Shu, E. Tadmor (Editor-in-Chief: A. Quarteroni) (Eds.), Advanced Numerical Approximation of Nonlinear Hyperbolic Equations, Lecture Notes in Mathematics 1697, Springer, Berlin, 1998, pp. 325–432.

[20] G. Cavallaro, C. Marchioro, On the approach to equilibrium for a pendulum immersed in a stokes fluid, Math. Models Methods Appl. Sci. **20**, 1999–2019 (2010).